Cold Adaptation of Enzyme Reaction Rates[†]

Sinisa Bjelic,[‡] Bjørn O. Brandsdal,[§] and Johan Åqvist*[,‡]

Department of Cell and Molecular Biology, Uppsala University Biomedical Center, Box 596, SE-751 24 Uppsala, Sweden, and Norwegian Structural Biology Center, Department of Chemistry, University of Tromsø, N-9037 Tromsø, Norway

Received June 24, 2008; Revised Manuscript Received August 13, 2008

ABSTRACT: A major issue for organisms living at extreme temperatures is to preserve both stability and activity of their enzymes. Cold-adapted enzymes generally have a reduced thermal stability, to counteract freezing, and show a lower enthalpy and a more negative entropy of activation compared to mesophilic and thermophilic homologues. Such a balance of thermodynamic activation parameters can make the reaction rate decrease more linearly, rather than exponentially, as the temperature is lowered, but the structural basis for rate optimization toward low working temperatures remains unclear. In order to computationally address this problem, it is clear that reaction simulations rather than standard molecular dynamics calculations are needed. We have thus carried out extensive computer simulations of the keto−enol(ate) isomerization steps in differently adapted citrate synthases to explore the structure−function relationships behind catalytic rate adaptation to different temperatures. The calculations reproduce the absolute rates of the psychrophilic and mesophilic enzymes at 300 K, as well as the lower enthalpy and more negative entropy of activation of the cold-adapted enzyme, where the latter simulation result is obtained from high-precision Arrhenius plots. The overall catalytic effect originates from electrostatic stabilization of the transition state and enolate and the reduction of reorganization free energy. The simulations, however, show psychrophilic, mesophilic, and hyperthermophilic citrate synthases to have increasingly stronger electrostatic stabilization of the transition state, while the energetic penalty in terms of internal protein interactions follows the reverse order with the cold-adapted enzyme having the most favorable energy term. The lower activation enthalpy and more negative activation entropy observed for cold-adapted enzymes are found to be associated with a decreased protein stiffness. The origin of this effect is, however, not localized to the active site but to other regions of the protein structure.

Adaptation of enzyme kinetics and protein stability is essential for the survival of organisms living under extreme temperature conditions. Enzymes working in cold environments have a reduced thermal stability compared to their mesophilic homologues to counteract freezing (*1*−*3*). Another characteristic property of cold-adapted enzymes is that their catalyzed reactions generally have lower activation enthalpies and more negative activation entropies than mesophilic and thermophilic homologues with similar activation free energies (*1*−*3*). This apppears to be a key feature of cold adaptation since it can provide a remedy for the exponential damping of the rate at lower temperatures that would follow from a high activation enthalpy. This enthalpy−entropy balance has been proposed to originate from a higher active site flexibility of cold-adapted enzymes (*1, 2, 4*), although there seems yet to be no strong experimental support for this hypothesis. Recent theoretical results (*5*), on the other hand, suggest that fluctuations along the chemical reaction coordinate are similar for mesophilic and thermophilic dihydrofolate reductases in the reactant state. Furthermore, while folding/unfolding motions were found to be more restricted in the thermophilic enzyme, these tended to be uncorrelated (orthogonal) to motions along the chemical reaction coordinate (*5*). In the case of psychrophilic uracil−DNA glycosylase, molecular dynamics simulations have indicated that the enzyme has a higher flexibility in the DNA recognition loop than its mesophilic equivalent (*6*), but the possible relation to catalytic rate is not clear. Due to their interrelation, it is difficult in general to distinguish temperature adaptation effects on catalytic rates, *per se*, from those that mainly have to do with thermal stability.

Electrostatic interactions have also been proposed to be important for cold adaptation, in the case of citrate synthase, but rather through destabilizing effects on the enzyme structure that presumably would counteract freezing (*7, 8*). Other suggested structural solutions for improving the catalytic efficiency at low temperatures are increased size and better accessibility of the active site, which would facilitate diffusional entry and exit of substrate and products (*1*). While this may seem consistent with the structure of cold-adapted citrate synthase (*9*), mutational studies have demonstrated that accessibility is not a major factor in increasing catalytic activity of this enzyme (*10*). The same study also showed the unexpected result that a loop insertion

[†] This work was supported by a grant from the Swedish Research Council (VR) and by computational resources provided by SNIC and UPPMAX. The Norwegian Structural Biology Center is supported by the Functional Genomics Program (FUGE) of the Research Council of Norway.

* Corresponding author. Phone: +46 18 471 4109. Fax: +46 18 53 69 71. E-mail: aqvist@xray.bmc.uu.se.

[‡] Uppsala University Biomedical Center.

[§] University of Tromsø.

10.1021/bi801177k CCC: $40.75
Published on Web 08/30/2008

into the cold-active enzyme yielded an increased thermostability but a reduced temperature optimum for catalytic activity.

The question of what are the main structure−function relationships behind catalytic rate optimization in cold-adapted enzymes thus largely remains unanswered, and to make progress, comparative analyses of the microscopic energetics of catalytic reactions from differently adapted homologous enzymes are required. Here, we employ extensive molecular dynamics (MD)[1] free energy simulations in combination with the empirical valence bond (EVB) method (*11, 12*) to examine the reactions of psychrophilic and mesophilic citrate synthase, along with some results also for a hyperthermophilic variant. In order for such reaction simulations to be informative, it is not only necessary that they reproduce experimental rates at given temperatures but also necessary that they reproduce the experimentally verified trends regarding activation entropy and enthalpy. We have thus carried out extensive calculations at five to six different temperatures in order to obtain Arrhenius plots of sufficient accuracy for both the psychrophilic and mesophilic enzymes. To the best of our knowledge, this is the first time that reliable estimates of enzyme thermodynamic activation parameters have been obtained using this approach.

Citrate synthase (CS) is part of the citric acid cycle and has been extensively studied, with X-ray structures determined from psychrophiles (*9*), mesophiles (*13*), and thermophiles (*7*). These enzymes are active as dimers of identical subunits, and the substrates acetyl-coenzyme A (AcCoA) and oxaloacetate (OAA) bind to an open form that closes upon binding (*14*). Both subunits are catalytically active and convert, through a Claisen-type condensation reaction, substrates to citrate and coenzyme A (*14*). The reaction is initiated by a proton abstraction from the aliphatic carbon of the acetyl group of AcCoA by an aspartate residue, and this process has been found to be rate-limiting for the mesophilic *Sus scrofa* (pig) CS reaction (*15*). The cold-adapted *Arthobacter* DS2-3R and pig enzymes have similar rates at 300 K, while the latter enzyme is considerably more efficient at higher temperatures and the former more active at lower temperatures (*16*). We will thus focus here on the initial keto−enol(ate) isomerization step, which is an intrinsically slow prototypic type of reaction catalyzed by a number of different enzymes (*17, 18*). The overall mechanism of mesophilic citrate synthase has also been extensively studied previously with different quantum mechanical/molecular mechanics (QM/MM) methods (*19*−*24*) and can be considered well established.

MATERIALS AND METHODS

EVB Reaction Surface. The enolization reaction was described with the EVB method (*11, 12*) as an interconversion between two different resonance structures, Φ_i, describing the reactant and enolate states of the reaction. Each resonance form is represented by a specific potential energy function, ε_i, that determines the energetics associated with that structure. Atoms included in the EVB model of the reacting region consisted of the side chain of the catalytic aspartate and the acetyl-coenzyme A as far as the sp^3 carbon adjacent to the thio group. The EVB potential surface is fitted to available experimental or *ab initio* data regarding the uncatalyzed reaction in solution by adjusting the off-diagonal terms H_{ij} as well as the gas phase energy shifts α^i (*11, 12*).

A suitable water reaction for parametrization of the first citrate synthase reaction step is the proton abstraction from ethyl thioacetate by acetate. The activation and reaction free energy were estimated for this reaction in a 1 M standard state according to the free energy relationship in refs *25* and *26* to be 29.5 and 22.9 kcal/mol, respectively, where the values are corrected for the number of equivalent protons. The predicted reaction energetics agree well with experimentally determined reactions with stronger bases than acetate, such as hydroxide ion and 3-quinuclidone, that abstract the proton from ethyl thioacetate with activation energies (reaction rates) of ~20 kcal/mol (0.007 s^{-1}) and ~24 kcal/mol (0.00002 s^{-1}), respectively (*27, 28*). The rate for the uncatalyzed water reaction was further corrected by the entropic factor of *RT* ln 55 that is required for bringing the reacting atoms from a 1 M concentration to contact distance in aqueous solution (*11, 29, 30*). The final activation and reaction free energies that were used for parametrization of water reaction were thus 27.1 and 22.9 kcal/mol, respectively. These experimental values were reproduced in water by adjusting the relevant EVB parameters (*11, 12*) to $\Delta\alpha = 62.9$ kcal/mol and $H_{12} = 66.0$ kcal/mol.

Spherical Boundary Simulations. Dimers of the psychrophilic, mesophilic, and hyperthermophilic citrate synthases were constructed from crystallographic structures with PDB codes 1A58, 2CTS, and 1AJ8 (*9, 13, 31*). The substrates AcCoA and OAA were built from the preexisting ligands. All MD simulations were carried out with the molecular dynamics package Q (*32*) utilizing the Amber95 force field (*33*). Partial charges for AcCoA were derived from ref *19*, and OAA atomic charges were determined in accordance with the prescription for the Amber95 force field (*33*). A simulation sphere radius of 25.5 Å was centered on OAA and solvated with TIP3P water molecules (*34*). Residues outside the sphere were harmonically restrained by 100 kcal·mol^{-1}·Å^{-2} and excluded from nonbonded calculations. Atoms within a 5 Å shell from the sphere boundary were restrained by 25 kcal·mol^{-1}·Å^{-2} to provide a buffer region between tightly restrained and fully mobile atoms. Nonbonded van der Waals interactions were truncated beyond a 10 Å cutoff, while long-range electrostatics beyond this cutoff were treated by the LRF method (*35*). No cutoff was applied for any interactions involving atoms in the EVB region. The total charge inside the simulation sphere was −1 for all three enzymes. Water molecules close to the sphere surface were subjected to radial and polarization restraints (*32, 36*).

Each enzyme and water reaction free energy profile involved 300 ps of MD simulation with a time step of 1 fs and comprised 41 discrete FEP steps. The Arrhenius plots determined for CS^p and CS^m were based on five and six different temperatures, respectively, and at each temperature point between 38 and 65 independent FEP simulations were carried out, while the free energy profile for CS^h at 300 K was based on 11 independent simulations. In addition, longer MD averages for the three

[1] Abbreviations: MD, molecular dynamics; FEP, free energy perturbation; EVB, empirical valence bond; CS, citrate synthase; AcCoA, acetyl-coenzyme A; OAA, oxaloacetate; CS^p, psychrophilic citrate synthase; CS^m, mesophilic citrate synthase; CS^h, hyperthermophilic citrate synthase.

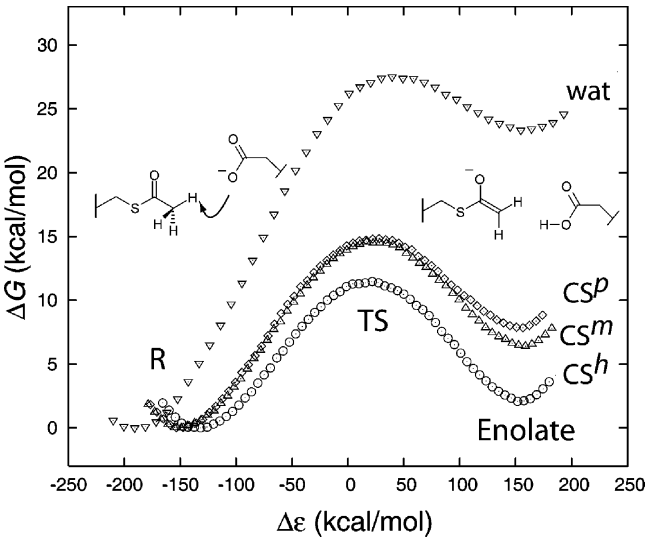

FIGURE 1: Calculated free energy profiles for the enolate formation step in psychrophilic (CS^p), mesophilic (CS^m), and hyperthermophilic (CS^h) citrate synthases together with the corresponding free energy profile for the uncatalyzed water reaction (upper curve). R denotes reactants, TS denotes transition state, and $\Delta\varepsilon$ is the generalized reaction coordinate (*11, 12*).

enzymes at 300 K in the reactant and transition state were calculated from 12 ns trajectories. Overall, the accumulated simulation time was well over 100 ns.

Periodic Boundary Simulations. MD simulations were carried out in the reactant state using the Amber9 program package (*37*) and the Amber95 force field (*33*). The citrate synthase dimers were solvated with TIP3P (*34*) water in a box with a volume of $\sim 130 \times 110 \times 100$ Å^3 that finally contained ~130000 atoms. Counterions were added to obtain neutral systems. The particle mesh Ewald method (*38*) was used to treat long-range electrostatics. Bonds involving hydrogens were constrained with SHAKE (*39*) to allow a time step of 2 fs. Before simulations, the initial coordinates were minimized with steepest decent and conjugate gradients algorithms. After minimization, the temperature was increased from 1 to 300 K under constant volume in 50 ps, followed by 500 ps constant pressure simulation. The systems were then simulated for 4.5 ns at 1 atm and 300 K.

RESULTS AND DISCUSSION

Catalysis at 300 K. Computer simulations of the enolate formation process were carried out for the mesophilic citrate synthase (CS^m) from *S. scrofa* (pig), the psycrophilic enzyme (CS^p) from DS2-3R, and hyperthermophilic enzyme (CS^h) from *Pyrococcus furiosus*. We will mostly focus on the two former enzymes, since the experimental data for these allow more direct comparisons (see below). The three enzymes have optimal working temperatures of 31 °C (CS^p), 55 °C (CS^m), and 91 °C (CS^h) (*16, 40*). The calculations utilized MD/EVB simulations together with the free energy perturbation (FEP)/umbrella sampling method (*11, 12*) and were averaged over up to 65 independent runs in order to obtain accurate reaction free energy profiles. Figure 1 shows the calculated free energy along the reaction coordinate for this process in the three enzymes together with the corresponding profile for the uncatalyzed enolate formation reaction in water. The simulations clearly show a large catalytic effect on this reaction step in all three enzymes, with stabilization of the transition state by more than 13 kcal/mol compared to water. The calculated free energy barriers of 14.1 ± 0.2 kcal/mol and 14.2 ± 0.2 kcal/mol (at 300 K) for CS^m and CS^p, respectively, are in excellent agreement with a barrier of ~15 kcal/mol estimated from the experimental rates at 300 K, $k_{cat}(CS^m) = 61\ s^{-1}$ and $k_{cat}(CS^p) = 42\ s^{-1}$ (*16*). The corresponding calculated activation energy for CS^h of 11.4 ± 0.1 kcal/mol is considerably lower, but there are no experimental rates available for this enzyme at 300 K. It is also likely that the subsequent reaction steps are rate-limiting in this case, as has been demonstrated for the thermostable citrate synthase from *Thermoplasma acidophilum* (*15*). However, even if other reaction steps are rate-limiting in some citrate synthases, it seems likely that the catalytic efficiency of the initial enolate formation reaction will be related to that of subsequent steps (*24*).

The active sites of the psychrophilic, mesophilic, and hyperthermophilic citrate synthases are very similar, and all of them stabilize the transient enolate intermediate directly through hydrogen bonding to a neutral histidine residue (His274 in CS^m) and a conserved water molecule (wat 1) as can be seen from the structures of the transient enolate intermediate in Figure 2. The protonated catalytic aspartic acid, Asp375 in CS^m, interacts similarly with the partially negative enolate α-carbon and accepts additional hydrogen bonds from Asn278 and another structurally conserved water molecule. In addition, three arginines and two histidines (Arg329, Arg401, Arg421, His238, and His320 in CS^m) that are involved in OAA binding also provide stabilizing interactions with the negative enolate. The same hydrogen-bonding pattern is found in CS^p and CS^h, except that the residue donating a hydrogen bond to the catalytic aspartate is instead a tyrosine residue (Tyr183 and Tyr185 in CS^p and CS^h, respectively). Previous theoretical calculations have shown that protonation of the enolate is generally unfavorable and that the enolate directly attacks oxaloacetate in the subsequent reaction step (*19*−*24*).

Temperature Dependence of Rates. In order to attack the problem of separating the enzymic free energy barriers into entropic and enthalpic contributions, we calculated free energy profiles at five to six different temperatures in the range of 280−300 K for CS^p and 285−320 K for CS^m. It is generally difficult to obtain sufficiently accurate Arrhenius plots from molecular dynamics free energy simulations, and this is probably the reason why no such calculations have yet been reported for any enzyme reaction. Here, we carried out 38−65 independent MD/FEP/EVB simulations at each of the temperature points, for each enzyme, in order to be able to reduce the error bars to an acceptable level. The resulting standard errors for the free energies are 0.1−0.2 kcal/mol (overall, these calculations required almost 100 ns of simulation time). The resulting Arrhenius plots are shown in Figure 3, where it can immediately be seen that the psychrophilic enzyme (CS^p) has a significantly smaller slope than the mesophilic one (CS^m). The calculated activation parameters for CS^p are $\Delta H^{\ddagger} = 7.4$ kcal/mol and $\Delta S^{\ddagger} = -22.7$ eu, while those for CS^m are $\Delta H^{\ddagger} = 11.5$ kcal/mol and $\Delta S^{\ddagger} = -9.7$ eu.

The simulations thus predict that the psychrophilic enzyme indeed has a lower activation enthalpy and a considerably more negative activation entropy than the corresponding

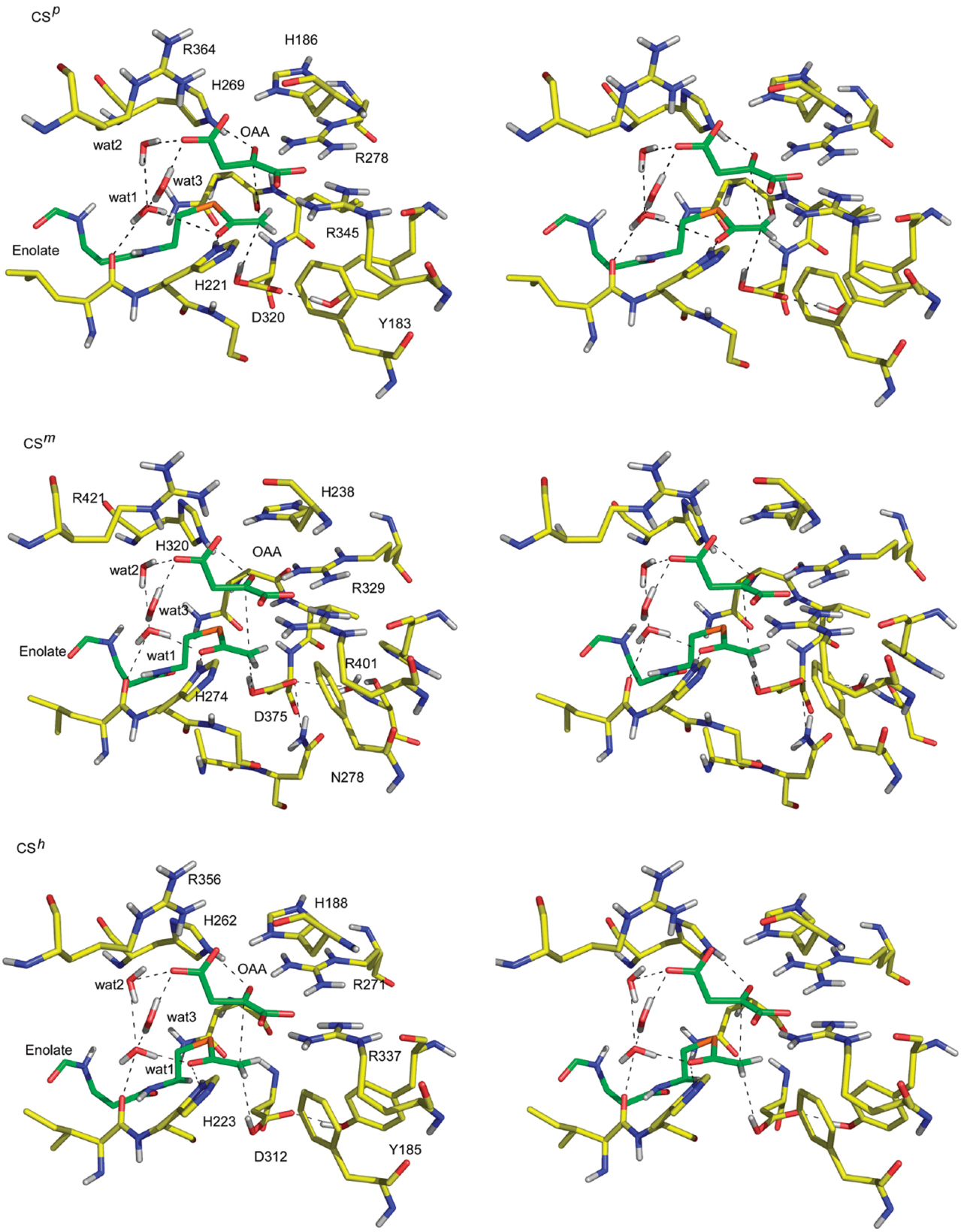

FIGURE 2: Stereoviews from MD simulations of the active sites of the psychrophilic, mesophilic, and hyperthermophilic citrate synthases in the enolate state. The structures are very similar, and the main differences involve interactions with the catalytic aspartate, i.e., a water molecule in CS^m compared to tyrosines Y183 and Y185 in CS^p and in CS^h, respectively. The oxaloacetate and part of the enolate intermediate of acetyl-coenzyme A are colored green.

mesophilic enzyme, as is usually found for cold-adapted enzymes (*4*). This result is also in good agreement with the temperature dependence of the activities that have been measured for the DS2-3R and pig enzymes (*16*), although no detailed activation parameters were given in ref *16*. Hence, the fact that both the absolute rates at 300 K and the different balance between activation enthalpy and entropy are reproduced for these two enzymes is very encouraging and allows

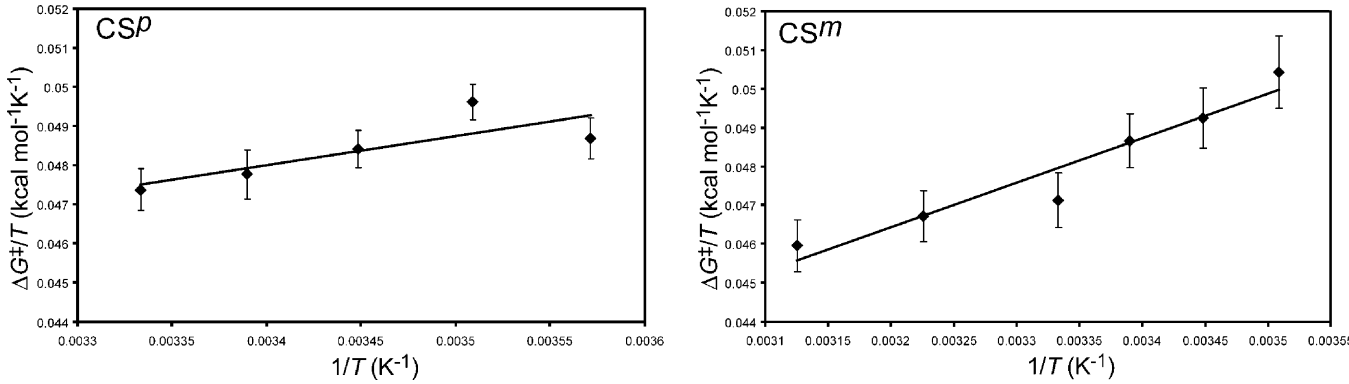

FIGURE 3: Calculated Arrhenius plots ($\Delta G^{\ddagger}/T$ vs $1/T$) for the enolate formation reaction in the psychrophilic (left) and mesophilic (right) citrate synthase. The clear difference in slopes demonstrates that CS^p has a lower activation enthalpy than CS^m.

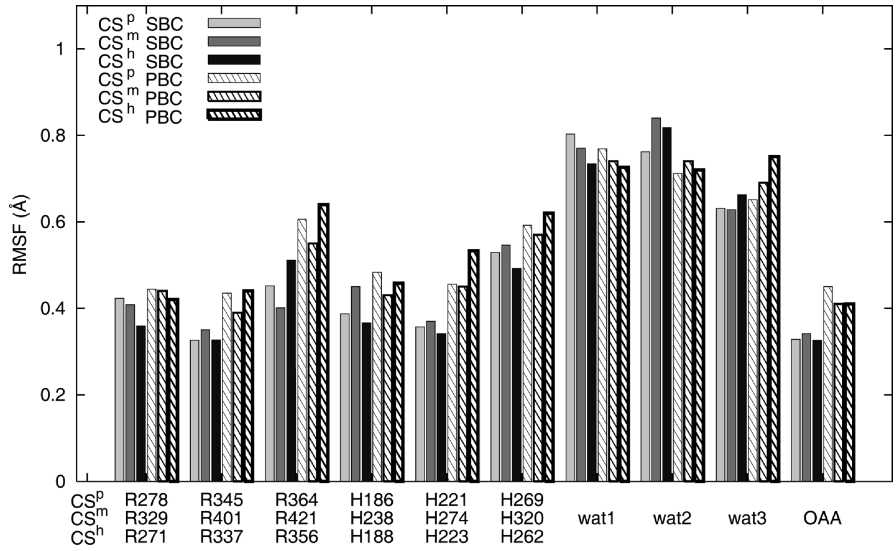

FIGURE 4: Active site RMSFs from molecular dynamics simulations using spherical and periodic boundary conditions (SBC and PBC, respectively) for the psychrophilic, mesophilic, and thermophilic citrate synthases. The amino acid residue numbering corresponds to the 1A59 (CS^p), 2CTS (CS^m), and 1AJ8 (CS^h) structures (cf. Figure 2).

us to search for the origin of this key characteristic difference between cold- and heat-adapted enzymes.

Active Site Flexibility. It has often been assumed that since cold-adapted enzymes benefit from higher flexibility, which counteracts freezing, and since the activation entropy is more negative, this could be interpreted in terms of an *increased flexibility of the active site* in the reactant or ground state (*4*). While a full dynamical analysis of the CS reaction cycle (including, e.g., opening−closing transitions) is beyond the scope of the present work, it is important to examine the idea of increased active site flexibility. In order to examine this proposal in the case of citrate synthases, we evaluated the root-mean-square fluctuations (RMSF) of the key residues surrounding the reactants in the active sites of all three enzymes, CS^p, CS^m, and CS^h. This was done using both the truncated spherical boundary model (with a 25.5 Å radius) employed in the MD/FEP/EVB simulations and using a much larger simulation system with periodic boundary conditions (PBC), that contained the entire dimeric enzyme and a total of about 130000 atoms. The RMSFs where thus determined for the three arginines, three histidines, oxaloacetate, and three water molecules that interact with the reacting groups, and these residues/molecules are common for all three homologues of citrate synthase.

The resulting plot of mobilities is shown in Figure 4, and as can be directly seen, there is no tendency for the psychrophilic enzyme to have larger active site RMSFs than the mesophilic and hyperthermophilic homologues. On the contrary, the positional fluctuations are extraordinarily similar in magnitude for the three enzymes, and the fact that the active site residues all have RMSFs below about 0.6 Å indicates that the site is rather rigid. This result is also in agreement with the experimental *B*-factors for CS^p that indicate RMSFs that are generally below 0.6 Å for the active site residues (*9*). Another striking feature of Figure 4 is that the simulations with spherical and periodic boundary conditions yield very similar results for the active site fluctuations. This shows that the mobility of the active site is not significantly damped by the spherical model, provided that its radius is sufficiently large (*41*). Hence, the results from analysis of the active site mobility with two different models are consistent and give no support for the idea that this region of the protein has an enhanced flexibility in the cold-adapted enzyme. This does, however, not mean that one can rule out possible effects of more global protein flexibility on cold adaptation of catalytic rates. That is, differences in mobility may be located to other regions of the enzyme where their main (but perhaps not sole) effect is to tune the thermal stability of the protein. We will return to this issue below.

Active Site Electrostatics. To understand the energetic origin of the large catalytic effect in the citrate synthases and whether contributions to it differ between the differently

Table 1: Partitioning of the Average EVB Activation Potential Energy (in kcal/mol) in Citrate Synthases

energy[a]	$\Delta U^{\ddagger}_{rr+rs,el}$	$\Delta U^{\ddagger}_{rs,el}$	$\Delta U^{\ddagger}_{rr,el}$	$\Delta U^{\ddagger}_{vdW}$	$\Delta U^{\ddagger}_{bnd}$	$\Delta U^{\ddagger}_{ang}$	$\Delta U^{\ddagger}_{tor}$	$\Delta U^{\ddagger}_{imp}$	$\Delta U^{\ddagger}_{rr+rs}$
water	-9.2 ± 2.3	29.7	-38.8	18.6	16.3	5.2	-0.2	-1.0	29.6
CS^p	-27.7 ± 0.9 (-27.7)	10.8	-38.4	17.6	17.4	4.6	0.1	-1.3	10.7
CS^m	-32.5 ± 1.5 (-30.8)	4.3	-36.8	18.2	18.6	4.6	-0.2	-1.2	7.6
CS^h	-37.0 ± 1.6 (-35.8)	0.3	-37.2	16.6	19.1	5.3	-1.3	-0.9	1.8

[a] Energy (ΔU) components: el, electrostatic; vdW, van der Waals; bnd, bond, ang, angle; tor, torsion; imp, improper. Subscripts rr and rs denote interactions among the atoms in the EVB region and between the EVB region and the surroundings, respectively. Values within parentheses are averages from several additional nanosecond long simulations at reactant and transition states.

adapted enzymes, it is useful to examine energy components associated with transition state stabilization. Table 1 shows a breakdown of the average potential energy change, between reactants (ground state) and transition state, for the reacting groups in each enzyme and for the uncatalyzed reaction in water. This quantity, $\Delta U^{\ddagger}_{rr+rs}$, contains contributions from interactions among the reacting atoms and from interactions between the reacting region and the surroundings (the indices r and s denote the reacting groups and their surroundings, respectively). It can be seen that all three enzymes cause a considerable reduction of $\Delta U^{\ddagger}_{rr+rs}$ compared to the water reaction, with a clear correlation between the magnitude of this reduction and the optimal working temperature of the enzyme. Hence, the hyperthermophilic enzyme shows the largest stabilization while the psychrophilic CS^p is most "water-like". It is also clear that neither bonded energy terms nor van der Waals interactions make any significant contribution to the reduction of $\Delta U^{\ddagger}_{rr+rs}$. Instead, the entire effect originates from electrostatics and, more specifically, from the electrostatic interactions between the reacting groups and the protein/water surroundings. Hence, the corresponding average electrostatic energy terms $\Delta U^{\ddagger}_{rr+rs,el}$ follow the same trend as $\Delta U^{\ddagger}_{rr+rs}$ and show that the higher the enzyme working temperature, the larger the electrostatic contribution to transition state stabilization. In order to further verify this result, we carried out additional long simulations (24 ns) for each system, as an alternative to the approach with many independent trajectories, and these results confirm our conclusions (data shown within parentheses in Table 1).

It is noteworthy that the three enzymes are able to reduce the electrostatic potential energy difference between transition state and reactants by 18−28 kcal/mol compared to water. The residues giving the most favorable contributions to $\Delta U^{\ddagger}_{rr+rs,el}$ in all three enzymes are found to be His274 (−9.4), Wat1 (−5.6), Arg421B (−5.3), His238 (−5.1), Arg401 (−5.0), and Arg329 (−4.4), with energies (in kcal/mol) from the CS^m simulations within parentheses. These results are also in general agreement with the calculations of Mulholland and co-workers (*20, 21*). Here, it is important to point out that interactions with the above-mentioned active site residues are similar in all three enzymes and not responsible for the differences in the electrostatic term. Figure 5 shows a partitioning of the contributions to $\Delta U^{\ddagger}_{rr+rs,el}$ from the interactions with the surroundings, $\Delta U^{\ddagger}_{rs,el}$, obtained from the long simulation averages. There it can be seen that the OAA and AcCoA molecules both give positive contributions to $\Delta U^{\ddagger}_{rs,el}$, due to their negative charges, and that this destabilization is very similar for all enzymes. The total contribution from the protein is clearly more favorable in CS^m and CS^h than in CS^p, and the difference can be seen to mainly derive from subunit B. The interactions with solvent further favor CS^h over CS^m, yielding a total ranking of the $\Delta U^{\ddagger}_{rs,el}$ terms

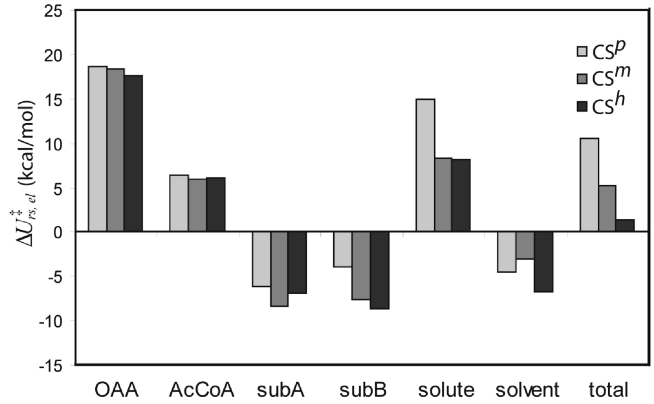

FIGURE 5: Partitioning of the electrostatic interaction energy between the reacting region and the surroundings, based on the long simulation averages. The electrostatic transition state stabilization, $\Delta U^{\ddagger}_{rs,el}$, becomes more negative when going from cold- to heat-adapted enzymes. $\Delta U^{\ddagger}_{rs,el}$ is calculated as a difference between the transition and reactant states, excluding intra-EVB-region interactions, $\Delta U^{\ddagger}_{rr,el}$. The two subunits are denoted subA and subB, where the reaction occurs in the former. Solute denotes the sum of electrostatic interactions for OAA, AcCoA, subA, and subB.

in accordance with Table 1 (note that the $\Delta U^{\ddagger}_{rr,el}$ interactions which in all cases are −37 to −38 kcal/mol have been excluded from Figure 5). It should, however, be pointed out that the separation of solute and solvent contributions in Figure 5 is somewhat misleading since mutations of a larger side chain to a smaller side chain often can allow the entry of additional water molecules that could be regarded as part of the protein. It is thus the overall effect of the electrostatic stabilization that matters, and our main conclusion here is that this quantity is clearly correlated with the cold-heat scale of enzyme adaptation.

Relation between $\Delta H^{\ddagger}$, $\Delta S^{\ddagger}$, *and* $\Delta U^{\ddagger}_{rs,el}$. The results from Arrhenius plots showed that $\Delta H^{\ddagger}$ is lower and $\Delta S^{\ddagger}$more negative for the psychrophilic enzyme than for the mesophilic homologue, in agreement with experiments, while $\Delta U^{\ddagger}_{rs,el}$ was found to be more positive. This implies that there is a positive correlation between $\Delta U^{\ddagger}_{rs,el}$ and the $-T\Delta S^{\ddagger}$ contribution to the free energy of activation. At first glance this may seem counterintuitive since one might expect a potential energy term such as $\Delta U^{\ddagger}_{rs,el}$ to be directly (positively) correlated to the enthalpy of activation, $\Delta H^{\ddagger}$. However, it is important to keep in mind that $\Delta H^{\ddagger}$ reflects the total potential energy change of the system (disregarding the $p\Delta V^{\ddagger}$ term):

$$\Delta H^{\ddagger} = \Delta U^{\ddagger}_{rr} + \Delta U^{\ddagger}_{rs} + \Delta U^{\ddagger}_{ss} \quad (1)$$

Hence, we have essentially three contributions to $\Delta H^{\ddagger}$ that originate from interactions (i) within and between the reacting groups, (ii) between these groups and the surrounding protein and water, and (iii) the interactions within the surroundings. Our calculations show that the first of these terms, $\Delta U^{\ddagger}_{rr}$, is

practically the same for all three enzymes and for the uncatalyzed water reaction, while $\Delta U^{\ddagger}_{rs}$ is significantly more positive for CS^p than CS^m and much more positive for the uncatalyzed reaction. Furthermore, the differences in $\Delta U^{\ddagger}_{rs}$ are completely dominated by electrostatic interactions. Hence, in order for the psychrophilic enzyme to have a lower overall $\Delta H^{\ddagger}$ than the mesophile, it must be the case that $\Delta U^{\ddagger}_{ss}$ is smaller. One may try to evaluate $\Delta U^{\ddagger}_{ss}$ from direct simulations, as was done by Trobro and Åqvist (*42*), but since this quantity involves a very large number of interactions (protein and water), convergence is usually slow (*42*). Here, we instead infer $\Delta U^{\ddagger}_{ss}$ from eq 1 since we have sufficiently accurate values of the other three terms. This shows that $\Delta U^{\ddagger}_{ss}$ is about 7 kcal/mol lower for CS^p than CS^m.

What does it mean that $\Delta U^{\ddagger}_{ss}$ is smaller for a psychrophilic than a mesophilic enzyme? First, it is reasonable to equate $\Delta U^{\ddagger}_{ss}$ to interactions within the protein, including internal water molecules, since the chemical rearrangements in the active site are not likely to cause significant changes in the solvation structure outside the protein (active sites are usually well shielded from the outside solvent). This would mean that it costs more energy in terms of protein−protein interactions, $\Delta U^{\ddagger}_{pp}$, to climb the activation barrier in a mesophilic (or thermophilic) enzyme than in a psychrophilic one, in spite of the fact that the interactions between the reaction groups and the enzyme ($\Delta U^{\ddagger}_{rs}$) are more favorable in the former case. This gives the immediate prediction or interpretation that the mesophilic enzyme has a larger degree of favorable preorganization toward the substrates but that this preorganization is associated with a stiffer or more rigid protein. The relation to protein stability thus appears to be the following: if you need a more rigid protein to counteract melting, this will require a better preorganization toward the transition state to maintain a given catalytic activity. Conversely, if you need to have a more flexible protein to counteract freezing, you will have to sacrifice some preorganization. However, the preorganization concept (*43*−*45*) is usually understood in terms of local active site structure, but here we are rather dealing with secondary effects outside the active site, since the active site is highly conserved between the enzymes and the key residues have virtually identical contributions to $\Delta U^{\ddagger}_{rs}$ and very similar RMSFs in CS^p and CS^m. The above analysis thus shows that there indeed is a relationship between enzyme rigidity or flexibility and the underlying enthalpic and entropic components of the activation free energy but that it is not localized to the active site. It should also be kept in mind that at 300 K both our calculations and experiments (*16*) show that CS^p and CS^m have more or less equal activities, illustrating that it is rather the temperature dependence than the magnitude of the catalytic effect that is related to protein flexibility. That is, the overall catalytic effect originates in all three citrate synthases from a similarly rigid and electrostatically preorganized active site, as is the case for many other enzymes (*44*). The preorganization term can also be evaluated quantitatively using the linear response approximation approach (*46*).

Mutations Affecting Energetics vs Flexibility. In view of the above discussion it is interesting to examine mutations between homologous enzymes adapted to different temperatures to see whether their effects can be understood. That is, can we say which mutations affect interactions with the transition state ($\Delta U^{\ddagger}_{rs}$) and which affect protein flexibility? From computer simulations of the present type the first task is rather straightforward, and by examining the contributions to $\Delta U^{\ddagger}_{rs}$ on a residue basis, one can try to identify hot spots that differ between the homologues. However, the total difference between two such enzymes may be the sum of many small contributions, particularly if the sequence identity is low. In our case, CS^p and CS^h have about 40% sequence identity, while CS^p and CS^m have only 30% identity (*9*), but nevertheless, some key regions can be identified. Hence, the N-terminal part of the α-helix (helix N) following the loop where His274 (CS^m numbering) is situated is found to provide a significant contribution to the $\Delta U^{\ddagger}_{rs+rr,el}$ trend in Table 1. Particularly the tripeptide sequence 278−280, which differs in all three enzymes, seems to be important for this effect, and these residues are just outside the active site. Another region that can be identified is the *β*-strand from the second subunit that is part of the dimer interface and carries Arg421 that makes contact with OAA. Here, Lys423 in CS^m and Arg358 in CS^h correspond to Leu366 in CS^p, and the loss of this positive charge removes a favorable interaction with the reacting groups, although it is a typical secondary interaction. Interestingly, this mutation also removes an intersubunit H-bond across the dimer interface, present in both CS^m and CS^h, and may therefore also have an effect on thermal stability.

There are also regions containing mutations that clearly affect mobility rather than energetics. One such example is around the N-terminal part of the surface-exposed α-helix (helix P) that covers the active site. Here the sequence corresponding to 324−331 in CS^m is dissimilar between the three enzymes with only two conserved residues. Both the SBC and PBC simulations show a considerable increase in both backbone and side chain RMSFs for CS^p in this region compared to CS^m and CS^h. Particularly, the substitutions at positions 326 and 331, where the psychrophilic enzyme has a glycine and proline residue, respectively, instead of two threonines in CS^m and a tyrosine and an arginine in CS^h, have increased backbone fluctuations by up 60% in CS^p. Another striking example is Val380 in CS^m that is located in helix R and is involved in the packing of the helix P, Q, and R termini, also at the protein surface. This residue is a leucine in CS^h, with somewhat lower backbone RMSFs compared to CS^m, but is changed to proline in the psychrophilic enzyme. With the proline in this position the backbone fluctuations are more than doubled compared to CS^m and CS^h, and the helix packing is also structurally affected, which clearly points to a role for enzyme stability of this residue. It should be pointed out here that the above mutations mainly affect mobility, with very little influence on $\Delta U^{\ddagger}_{rs}$. Figure 6 shows schematically the locations of the different "energetic" and "flexibility" mutations discussed, in the 3D structure of the mesophilic enzyme. This illustrates the general feature that emerges upon closer examination of the sequence differences showing effects on either energetics or flexibility, namely, that they tend not to be located in direct contact with the substrates but rather in a secondary layer, or even further away from them.

CONCLUDING REMARKS

We have focused here on the problem of cold adaptation of enzyme catalytic rates and used extensive computer

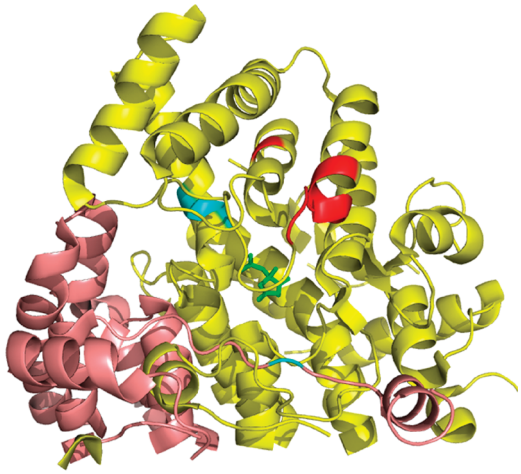

FIGURE 6: View of part of the CS^m dimer (subunits in yellow and pink ribbons) around one of the active sites with the crystallographic citrate molecule in green sticks. Key mutations affecting reaction energetics and mobility are colored in cyan and red, respectively.

simulations to explore the underlying energetics of this phenomenon. Cold adaptation of enzymes, or temperature adaptation in general, is a two-sided coin where a proper balance must be found between catalytic efficiency and thermal stability (*47*). The latter problem is much better understood, with regard to both how psychrophilic enzymes avoid freezing and how thermophilic ones avoid melting. However, the relations between factors that affect thermal stability and those that affect reaction rates do not appear as straightforward. While both enzyme flexibility and electrostatic interactions have been proposed to be important for cold adaptation of enzymic rates (*1, 2*), it has remained unclear what the actual mechanisms would be for acquiring a reasonable activation free energy at lower temperatures.

Our calculations on differently adapted citrate synthases reproduce the absolute rates for the psychrophilic and mesophilic enzymes, as well as the important property that cold-adapted enzymes generally have lower enthalpy and more negative entropy of activation than mesophilic counterparts with similar free energy barriers. The simulations show that the cold-adapted enzyme has less electrostatic stabilization of the transition state than the mesophilic and hyperthermophilic homologues but that it has a more favorable internal energy change of the protein which more than counterbalances the loss of electrostatic stabilization. It is, however, important to emphasize here that activation free energies of the psychrophilic and mesophilic enzymes are virtually identical at 300 K and that the origin of the catalytic effect resides in electrostatic stabilization of the transition state and enolate and the reduction of reorganization free energy, while its partitioning into enthalpy and entropy differs. It seems obvious that the internal protein−protein interactions here provide a connection to thermal stability, since a more heat-resistant protein would generally be stiffer and have a larger energetic penalty against conformational fluctuations. However, the present simulations show that neither the weakened electrostatic stabilization of the transition state nor the increased mobility in the psychrophilic enzyme is localized to the active site but is rather a more global effect originating from other regions of the protein. This seems to make sense indeed, since if one were to evolve a more heat-labile protein while maintaining catalytic efficiency, the active site itself would be an unwise choice for mutations.

ACKNOWLEDGMENT

We thank Prof. Måns Ehrenberg for useful comments.

REFERENCES

1. Feller, G., and Gerday, C. (2003) Psychrophilic enzymes: Hot topics in cold adaptation. *Nat. Rev. Microbiol. 1*, 200–208.
2. Siddiqui, K. S., and Cavicchioli, R. (2006) Cold-adapted enzymes. *Annu. Rev. Biochem. 75*, 403–433.
3. Fields, P. A., and Somero, G. N. (1998) Hot spots in cold adaptation: Localized increases in conformational flexibility in lactate dehydrogenase A_4 orthologs of Antarctic notothenioid fishes. *Proc. Natl. Acad. Sci. U.S.A. 95*, 11476–11481.
4. Lonhienne, T., Gerday, C., and Feller, G. (2000) Psychrophilic enzymes: revisiting the thermodynamic parameters of activation may explain local flexibility. *Biochim. Biophys. Acta 1543*, 1–10.
5. Roca, M., Liu, H., Messer, B., and Warshel, A. (2007) On the relationship between thermal stability and catalytic power of enzymes. *Biochemistry 46*, 15076–15088.
6. Olufsen, M., Smalås, A. O., Moe, E., and Brandsdal, B. O. (2005) Increased flexibility as a strategy for cold adaptation—A comparative molecular dynamics study of cold- and warm-active uracil DNA glycosylase. *J. Biol. Chem. 280*, 18042–18048.
7. Bell, G. S., Russell, R. J. M., Connaris, H., Hough, D. W., Danson, M. J., and Taylor, G. L. (2002) Stepwise adaptations of citrate synthase to survival at life's extremes—From psychrophile to hyperthermophile. *Eur. J. Biochem. 269*, 6250–6260.
8. Kumar, S., and Nussinov, R. (2004) Different roles of electrostatics in heat and in cold: Adaptation by citrate synthase. *ChemBioChem 5*, 280–290.
9. Russell, R. J. M., Gerike, U., Danson, M. J., Hough, D. W., and Taylor, G. L. (1998) Structural adaptations of the cold-active citrate synthase from an Antarctic bacterium. *Structure 6*, 351–361.
10. Gerike, U., Danson, M. J., and Hough, D. W. (2001) Cold-active citrate synthase: mutagenesis of active-site residues. *Protein Eng. 14*, 655–661.
11. Warshel, A. (1991) *Computer modeling of chemical reactions in enzymes and solutions*, John Wiley & Sons, New York.
12. Åqvist, J., and Warshel, A. (1993) Simulation of enzyme reactions using valence bond force fields and other hybrid quantum/classical approaches. *Chem. Rev. 93*, 2523–2544.
13. Remington, S., Wiegand, G., and Huber, R. (1982) Crystallographic refinement and atomic models of two different forms of citrate synthase at 2.7 and 1.7 Å resolution. *J. Mol. Biol. 158*, 111–152.
14. Wiegand, G., and Remington, S. J. (1986) Citrate synthase: Structure, control, and mechanism. *Annu. Rev. Biophys. Biophys. Chem. 15*, 97–117.
15. Kurz, L. C., Drysdale, G., Riley, M., Tomar, M. A., Chen, J., Russell, R. J. M., and Danson, M. J. (2000) Kinetics and mechanism of the citrate synthase from the thermophilic Archaeon *Thermoplasma acidophilum*. *Biochemistry 39*, 2283–2296.
16. Gerike, U., Danson, M. J., Russell, N. J., and Hough, D. W. (1997) Sequencing and expression of the gene encoding a cold-active citrate synthase from an Antarctic bacterium, strain DS2-3R. *Eur. J. Biochem. 248*, 49–57.
17. Feierberg, I., and Åqvist, J. (2002) Computational modeling of enzymatic keto-enol isomerization reactions. *Theor. Chem. Acc. 108*, 71–84.
18. Gerlt, J. A., and Gassman, P. G. (1993) An explanation for rapid enzyme-catalyzed proton abstraction from carbon acids: Importance of late transition states in concerted mechanisms. *J. Am. Chem. Soc. 115*, 11552–11568.
19. Donini, O., Darden, T., and Kollman, P. A. (2000) QM-FE calculations of aliphatic hydrogen abstraction in citrate synthase and in solution: Reproduction of the effect of enzyme catalysis and demonstration that an enolate rather than an enol is formed. *J. Am. Chem. Soc. 122*, 12270–12280.
20. Mulholland, A. J., and Richards, W. G. (1997) Acetyl-CoA enolization in citrate synthase: A quantum mechanical molecular mechanical (QM/MM) study. *Proteins: Struct., Funct., Genet. 27*, 9–25.

21. Mulholland, A. J., Lyne, P. D., and Karplus, M. (2000) Ab initio QM/MM study of the citrate synthase mechanism. A low-barrier hydrogen bond is not involved. *J. Am. Chem. Soc. 122*, 534–535.
22. van der Kamp, M. W., Perruccio, F., and Mulholland, A. J. (2007) Substrate polarization in enzyme catalysis: QM/MM analysis of the effect of oxaloacetate polarization on acetyl-CoA enolization in citrate synthase. *Proteins 69*, 521–535.
23. van der Kamp, M. W., Perruccio, F., and Mulholland, A. J. (2007) Ab initio QM/MM modelling of acetyl-CoA deprotonation in the enzyme citrate synthase. *J. Mol. Graphics Modell. 26*, 676–690.
24. van der Kamp, M. W., Perruccio, F., and Mulholland, A. J. (2008) High-level QM/MM modelling predicts an arginine as the acid in the condensation reaction catalysed by citrate synthase. *Chem. Commun. 16*, 1874–1876.
25. Åqvist, J., and Fothergill, M. (1996) Computer simulation of the triosephosphate isomerase catalyzed reaction. *J. Biol. Chem. 271*, 10010–10016.
26. Hegarty, A. F., and Jencks, W. P. (1975) Bifunctional catalysis of the enolization of acetone. *J. Am. Chem. Soc. 97*, 7188–7189.
27. Amyes, T. L., and Richard, J. P. (1992) Generation and stability of a simple thiol ester enolate in aqueous solution. *J. Am. Chem. Soc. 114*, 10297–10302.
28. Lienhard, G. E., and Wang, T. C. (1968) Kinetics of proton transfer from the α carbon of ethyl thioacetate and its dimethyliminium derivative. *J. Am. Chem. Soc. 90*, 3781–3787.
29. Bjelic, S., and Åqvist, J. (2004) Computational prediction of structure, substrate binding mode, mechanism, and rate for a malaria protease with a novel type of active site. *Biochemistry 43*, 14521–14528.
30. Strajbl, M., Florian, J., and Warshel, A. (2000) Ab initio evaluation of the potential surface for general base-catalyzed methanolysis of formamide: A reference solution reaction for studies of serine proteases. *J. Am. Chem. Soc. 122*, 5354–5366.
31. Russell, R. J. M., Ferguson, J. M. C., Hough, D. W., Danson, M. J., and Taylor, G. L. (1997) The crystal structure of citrate synthase from the hyperthermophilic Archaeon *Pyrococcus furiosus* at 1.9 Å resolution. *Biochemistry 36*, 9983–9994.
32. Marelius, J., Kolmodin, K., Feierberg, I., and Åqvist, J. (1998) Q: A molecular dynamics program for free energy calculations and empirical valence bond simulations in biomolecular systems. *J. Mol. Graphics Modell. 16*, 213–225.
33. Cornell, W. D., Cieplak, P., Bayly, C. I., Gould, I. R., Merz, K. M., Ferguson, D. M., Spellmeyer, D. C., Fox, T., Caldwell, J. W., and Kollman, P. A. (1995) A second generation force-field for the simulation of proteins, nucleic-acids, and organic molecules. *J. Am. Chem. Soc. 117*, 5179–5197.
34. Jorgensen, W., Chandrasekhar, J., Madura, J., Rw, I., and Klein, M. (1983) Comparison of simple potential functions for simulating liquid water. *J. Chem. Phys. 79*, 926–935.
35. Lee, F. S., and Warshel, A. (1992) A local reaction field method for fast evaluation of long-range electrostatic interactions in molecular simulations. *J. Chem. Phys. 97*, 3100–3107.
36. King, G., and Warshel, A. (1989) A surface constrained all-atom solvent model for effective simulations of polar solutions. *J. Chem. Phys. 91*, 3647–3661.
37. Pearlman, D. A., Case, D. A., Caldwell, J. W., Ross, W. S., Cheatham, T. E., Debolt, S., Ferguson, D., Seibel, G., and Kollman, P. (1995) AMBERr, a package of computer-programs for applying molecular mechanics, normal mode analysis, molecular dynamics and free energy calculations to simulate the structural and energetic properties of molecules. *Comput. Phys. Commun. 91*, 1–41.
38. Darden, T., York, D., and Pedersen, L. (1993) Particle mesh Ewald: An $N\cdot\log(N)$ method for Ewald sums in large systems. *J. Chem. Phys. 98*, 10089–10092.
39. Ryckaert, J. P., Ciccotti, G., and Berendsen, H. J. C. (1977) Numerical integration of the cartesian equations of motion of a system with constraints: Molecular dynamics of *n*-alkanes. *J. Comput. Phys. 23*, 327–341.
40. Arnott, M. A., Michael, R. A., Thompson, C. R., Hough, D. W., and Danson, M. J. (2000) Thermostability and thermoactivity of citrate synthases from the thermophilic and hyperthermophilic archaea, *Thermoplasma acidophilum* and *Pyrococcus furiosus*. *J. Mol. Biol. 304*, 657–668.
41. Almlöf, M., Brandsdal, B. O., and Åqvist, J. (2004) Binding affinity prediction with different force fields: Examination of the linear interaction energy method. *J. Comput. Chem. 25*, 1242–1254.
42. Trobro, S., and Åqvist, J. (2005) Mechanism of peptide bond synthesis on the ribosome. *Proc. Natl. Acad. Sci. U.S.A. 102*, 12395–12400.
43. Warshel, A. (1978) Energetics of enzyme catalysis. *Proc. Natl. Acad. Sci. U.S.A. 75*, 5250–5254.
44. Warshel, A. (1998) Electrostatic origin of the catalytic power of enzymes and the role of preorganized active sites. *J. Biol. Chem. 273*, 27035–27038.
45. Cannon, W. R., and Benkovic, S. J. (1998) Solvation, reorganization energy, and biological catalysis. *J. Biol. Chem. 273*, 26257–26260.
46. Warshel, A., Sharma, P. K., Chu, Z. T., and Åqvist, J. (2007) Electrostatic contributions to binding of transition state analogues can be very different from the corresponding contributions to catalysis: Phenolates binding to the oxyanion hole of ketosteroid isomerase. *Biochemistry 46*, 1466–1476.
47. Shoichet, B. K., Baase, W. A., Kuroki, R., and Matthews, B. W. (1995) A relationship between protein stability and protein function. *Proc. Natl. Acad. Sci. U.S.A. 92*, 452–456.

BI801177K